Earthline Journal of Chemical Sciences
E-ISSN: 2581-9003; CODEN: EJCSB4
Volume 12, Number 2, 2025, Pages 179-191
https://doi.org/10.34198/ejcs.12225.179191

Biogenic mediated synthesis, characterization, antimicrobial and radical scavenging studies of iron oxide nanoparticles (Fe_3O_4-NPs) using *Eichhornia crassipes* leaves extract

Abubakar Habib Idris*

Department of Chemistry, Abubakar Tafawa Balewa University, PMB 0248, Bauchi, Nigeria
e-mail: ahidris@atbu.edu.ng

Fartisincha Peingurta Andrew

School of Chemistry and Physics, University of KwaZulu-Natal, Private Bag X01, Scottsville, Pietermaritzburg, 3209, South Africa

Jamila Ibrahim Shekarau

Department of Chemistry, Abubakar Tafawa Balewa University, PMB 0248, Bauchi, Nigeria

Yasser Sabo Takko

Department of Chemistry, Abubakar Tafawa Balewa University, PMB 0248, Bauchi, Nigeria

Omolade Ojo

Department of Chemistry, Modibbo Adama University, PMB 2076, Yola, Nigeria

Aishatu Habib Idris

Department of Biological Science, Abubakar Tafawa Balewa University, PMB 0248, Bauchi, Nigeria

Abdullahi Aliyu

Department of Biological Science, Abubakar Tafawa Balewa University, PMB 0248, Bauchi, Nigeria

Aisha Khalida Haladu

Department of Chemistry, Abubakar Tafawa Balewa University, PMB 0248, Bauchi, Nigeria

Ibrahim Mohammed Warji

Department of Chemistry, Abubakar Tafawa Balewa University, PMB 0248, Bauchi, Nigeria

Abstract

The plant *Eichhornia crassipes* (commonly known as water hyacinth) was obtained from Lake Geriyo, Yola, Adamawa State, Nigeria. The sampled leaves were gently washed with deionized (DI) water and air-dried at room temperature (25–30 °C). Iron nanoparticles were synthesized using *Eichhornia crassipes* (water hyacinth extract) and characterized using XRD, SEM, TEM, SEM-EDX, and FTIR. The antioxidant activity of the iron nanoparticles was analyzed using DPPH scavenging activity.

The plant extracts and iron nanoparticles were tested for antibacterial efficiency against *Escherichia coli*, *Staphylococcus aureus*, *Streptococcus pneumoniae*, *Salmonella typhi*, and *Klebsiella pneumoniae*. The results

Received: February 14, 2025; Revised & Accepted: February 28, 2025; Published: March 18, 2025

Keywords and phrases: biogenic mediated, nanoparticles, water hyacinth, antimicrobial, antioxidant.

revealed the proximate composition of the water hyacinth plant, including moisture content, ash content, fiber, fat content, protein, and carbohydrates. The proximate composition followed the order: carbohydrates > lipids > fiber > moisture > protein > ash content.

Qualitative phytochemical screening of the leaf revealed the presence of carbohydrates, terpenoids, phenolics, and saponins, while amino acids, terpenes, alkaloids, steroids, and flavonoids were absent. SEM-EDX, TEM, XRD, and FTIR confirmed the formation of iron nanoparticles. The iron nanoparticles exhibited higher percentage inhibition with varied concentrations of 25% FeNPs, 50/50 FeNPs, and 25/75 FeNPs, with 25/75 FeNPs showing significant scavenging activity of 24%, 39%, 47%, 55%, and 73% at 10, 20, 30, 40, and 50 µl/ml, respectively.

The minimum inhibitory concentration (MIC) of 25% FeNPs for *Klebsiella pneumoniae* and *Staphylococcus aureus* showed that the extract had a higher inhibitory effect on *Klebsiella pneumoniae* compared to *Staphylococcus aureus*. The inhibition sequence showed similar inhibition for all pathogens except *Salmonella typhi* and *Klebsiella pneumoniae*, which exhibited the least inhibition among all FeNP concentrations. An increase in material concentration resulted in higher inhibition for four organisms, while *Klebsiella pneumoniae* showed a different trend, with the highest inhibition observed at a 200 µg/L concentration.

1. Introduction

In recent years, there has been a gradual emergence and increasing application of nanomaterials across various fields. This is primarily due to the unique properties of nanoparticles, such as their small size, large surface area-to-volume ratio, quantum effects, optical properties, and enhanced mechanical, magnetic, and thermal properties compared to bulk materials. Additionally, nanoparticles possess flexible surface chemistry, allowing for surface functionalization tailored to specific applications [1-5].

These distinctive properties make nanoparticles highly versatile and valuable for a wide range of applications in fields such as medicine, electronics, catalysis, environmental remediation, and materials science [6-9]. Among the many types of nanoparticles, iron oxide nanoparticles (Fe_3O_4-NPs) have garnered significant attention due to their unique superparamagnetic properties, large surface area-to-volume ratio, ease of synthesis, biocompatibility, low toxicity, and cost-effectiveness [9-14].

Several methods have been employed to synthesize Fe_3O_4-NPs, including hydrothermal [15], solvothermal [16], precipitation [17], and biogenic (also referred to as green synthesis) approaches. However, recent research has increasingly focused on green synthesis methods due to their cost-effectiveness, sustainability, and environmental friendliness. Various plant extracts, such as *Aloe vera* [18], *Moringa oleifera* [19], *Graptophyllum pictum* [20], and *Zanthoxylum armatum* [21], have been utilized for the green synthesis of nanoparticles.

Fe_3O_4-NPs have demonstrated varying degrees of biological activity against a range of pathogenic microbes, including bacteria [22], fungi [23], viruses [24], and protozoa [25]. Like most nanoparticles, Fe_3O_4-NPs exhibit unique mechanisms of action against microbial pathogens, including disruption of the cell membrane, interference with metabolic pathways, and generation of reactive oxygen species (ROS) [26-28].

Eichhornia crassipes, commonly known as water hyacinth, is an aquatic plant native to South America that has naturalized worldwide [29]. Since the 1800s, it has spread primarily to tropical and subtropical regions and is considered invasive due to its rapid growth beyond its native range. While water hyacinth has beneficial applications, such as phytoremediation and biomass production, its invasive nature poses significant environmental and socio-economic challenges. These include waterway obstruction, ecological disruption, habitat alteration, and water quality degradation [30, 31].

Despite its negative impacts, the plant has been reported to exhibit antibacterial, anti-inflammatory, and antifungal properties [32], as well as anti-aging [33] and anticancer activities [34].

In the pursuit of addressing the growing global concern of antimicrobial resistance, we report here the eco-friendly, biogenic-mediated synthesis of Fe_3O_4-NPs using varying concentrations of an iron solution and water hyacinth leaf extract. The nanoparticles were characterized using UV-Visible spectroscopy, X-ray diffraction (XRD), Fourier Transform Infrared (FTIR) spectroscopy, Scanning Electron Microscopy (SEM), and Transmission Electron Microscopy (TEM). Additionally, there in vitro antimicrobial activity was evaluated against *Staphylococcus aureus*, *Streptococcus pneumoniae*, *Escherichia coli*, *Salmonella typhi*, and *Klebsiella pneumoniae*, along with an assessment of their radical scavenging potential.

2. Materials and Methods

2.1. Extraction of the plant metabolite

The plant (*Eichhornia crassipes*, commonly known as water hyacinth) was obtained from Lake Geriyo, Yola, Adamawa State, Nigeria. The sampled leaves were gently washed with deionized (DI) water and air-dried at room temperature (25–30 °C). The dried leaves were then blended and sieved using a 200-mesh sieve (pore diameter: 0.074 mm). An aqueous extract of the plant leaves was prepared by boiling 10 g of the powdered leaves in 100 mL of DI water with continuous stirring for 10 minutes. The extract was then filtered and stored in a refrigerator for further use.

2.2. Synthesis of nanoparticles

Three different ratios—25 mL/75 mL, 50 mL/50 mL, and 75 mL/25 mL—of the plant extract and a 1 mM solution of iron (II, III) oxide (Fe_3O_4) were mixed and stirred at 80 °C for 1 hour. The resulting precipitate was then centrifuged, washed several times with water, and dried in a desiccator over silica

2.3. Characterization of the iron oxide (Fe_3O_4) nanoparticles

The spectroscopic analysis, namely UV-Visible spectroscopy, was performed using a Cary 60 spectrophotometer by Agilent Technologies. Fourier Transform Infrared (FTIR) spectroscopy was conducted using a Cary 630 spectrophotometer by Agilent Technologies. Morphological analysis, including scanning electron microscopy (SEM) and transmission electron microscopy (TEM), was carried out using the Phenom-ProX system. X-ray diffraction (XRD) analysis was performed using a MiniFlex 600 X-ray diffractometer.

2.4. Radical scavenging activity of the Fe_3O_4-NPs

The radical scavenging activity of Fe_3O_4-NPs was studied using the 1,1-Diphenyl-2-picrylhydrazyl (DPPH) method. In this method, 200, 400, 600, 800, and 1000 μL of the sample were taken in a series of test tubes, along with 1 mL of 100 μM DPPH solution dissolved in methanol. The mixture was adjusted to a final volume of 2 mL using methanol and incubated in the dark for 30 minutes to allow the reaction to occur. After incubation, the absorbance was measured using a UV-Vis spectrophotometer (UV-1800, Shimadzu) at a specific wavelength (nm).

In this experiment, methanol served as the blank, the DPPH solution without any test sample acted as the positive control, and ascorbic acid was used as the standard. The experiment was repeated three times, and the mean absorbance values were recorded. The inhibition percentage was determined using the following equation.

2.5. Antimicrobial studies

The antibacterial activities of all extracts of *Ziziphus spina-christi* and *Hymenocardia acida* were evaluated using the paper disc diffusion method [35]. Extended-spectrum beta-lactamase (ESBL)-producing *Pseudomonas aeruginosa* was first reactivated by inoculating it into freshly prepared peptone water and incubating it for 48 hours at 37 °C. The broth cultures of ESBL-producing *P. aeruginosa* were then adjusted to a 0.5 McFarland standard using a sterile 0.9% normal saline solution and inoculated onto cetrimide agar.

Sterilized filter paper discs (Whatman No. 1; 6 mm in diameter) were soaked in test tubes containing the dissolved extracts at different concentrations, picked up with sterilized forceps, air-dried, and placed on agar plates inoculated with the bacteria. The plates were then incubated for 24 hours at 37 °C.

The bacterial sensitivity or susceptibility to the standard drug was tested by placing discs seeded with amoxicillin-clavulanic acid (amoxy-clav, 20/10 μg) on each plate at different concentrations, serving as the positive control. Sterilized paper discs with dimethyl sulfoxide (DMSO) were used as negative controls for all plates. The experiment was performed in triplicate.

The bactericidal activity was determined by measuring the zone of inhibition around each paper disc. The results for the anti-*Pseudomonas* agent were compared with those of the plant extracts [36].

3. Results and discussion

3.1. Characterization

The structural characterization, phase analysis, and crystallinity of the synthesized samples were determined using the XRD technique with Cu Kα radiation (λ = 1.5406 Å) in the 2θ range of 20–80°, along with scanning electron microscopy (SEM).

3.2. Phytochemical and proximate analysis of the extract used as capping and reducing agent

Table 1 presents the qualitative phytochemical analysis, which revealed that the leaf extract of *Eichhornia crassipes* contains carbohydrates, terpenoids, phenolics, and saponins, while amino acids, terpenes, alkaloids, tannins, steroids, and flavonoids were absent. The proximate composition analysis of *Eichhornia crassipes* showed that carbohydrates had the highest composition, followed by lipids and then fiber, while ash content had the lowest value. The composition values followed the order:

Carbohydrates > Crude Lipid > Crude Fiber > Crude Protein > Moisture Content > Ash Content

Table 1. Phytochemical and proximate analysis of the plant extract.

Phytochemical screening of the plant extract		Proximate analysis of the plant extract	
Phytochemical component	**Aqueous extract**	**Parameter**	**% Composition**
Saponins	+	Moisture	10.06
Tannins	-	Ash content	7.41
Alkaloids	-	Crude fiber	14.92
Flavonoids	-	Crude lipid	21.75
Terpenoids	+	Crude protein	8.60
Steroids	-	Carbohydrates	36.72
Phenols	+		
Amino acids	-		
Carbohydrates	+		
Terpenes	-		

3.3. Fourier transform infrared spectroscopy

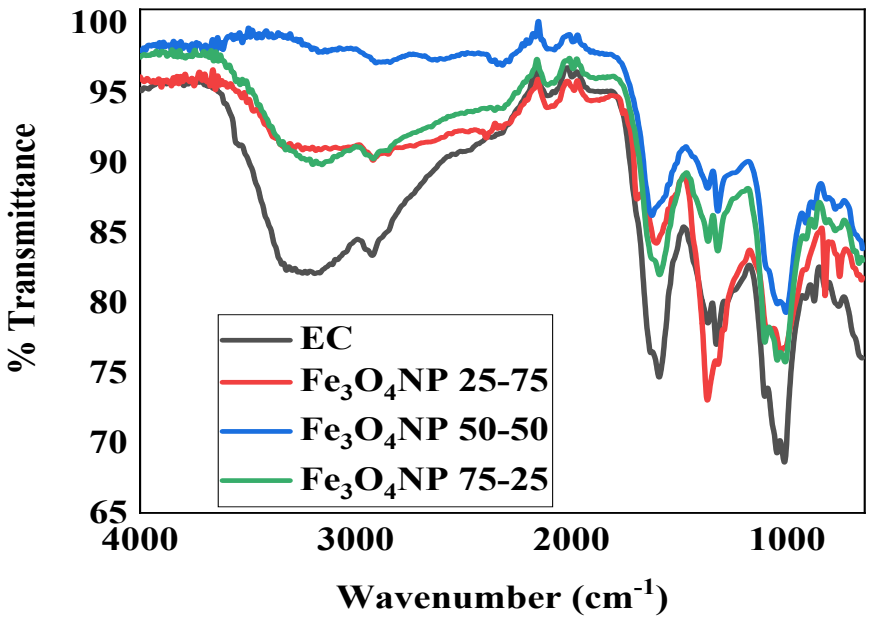

Figure 1. FTIR spectra of the extract and the Fe_3O_4-NPs.

The FTIR analysis of *Eichhornia crassipes* (EC) before synthesis is shown in Figure 1. The spectrum exhibits broad absorption spanning from 3100 to 3600 cm^{-1}, indicating the presence of O–H stretching vibrations. A peak at 3265 cm^{-1} corresponds to the alcohol functional group, while weak absorption at 2920 cm^{-1} is indicative of C–H stretching. The fingerprint region displays characteristic absorption peaks at 1600 cm^{-1}, 1313 cm^{-1}, and 1025 cm^{-1}, corresponding to nitro, alcohol, and amine functional groups, respectively. The presence of N–O, O–H, and C–N bonds suggests nitrogen-containing, alcohol-containing, and amine-containing metabolites in EC.

For a 25:75 ratio of iron oxide to EC, the FTIR analysis of the synthesized nanoparticles reveals

characteristic N–H stretching of aliphatic amines and C–C stretching of cyclic alkenes. N–O stretching at 1541 cm^{-1} and S–O stretching at 1030 cm^{-1} indicate functional groups typically found in iron oxide nanoparticles.

Vibrational frequencies observed at 3268 cm^{-1} and 1623 cm^{-1} suggest the presence of amine and alkene groups. A peak at 2920 cm^{-1} corresponds to thiols, while peaks at 1341 cm^{-1} and 1030 cm^{-1} indicate the presence of sulfoxide and sulfonamide functional groups.

For a 50:50 iron oxide-based nanoparticle composition, the FTIR spectrum exhibits similar peaks to the 75:25 iron oxide-to-extract nanoparticle ratio. Iron oxide interactions contribute to weak peaks observed at 1397 cm^{-1} and 1235 cm^{-1}. The synthesized nanoparticles display irregular peak patterns, differing from those observed in the extract prior to synthesis.

3.4. XRD-diffraction spectroscopy

The formation of the EC-Fe_3O_4NPs phase shift was confirmed by XRD analysis, as shown in Figure 2. The diffraction patterns reveal the presence of four distinct diffraction peaks. Strong peaks were observed at 2θ values of 26.34°, 29.92°, 38.02°, and 40.50°, corresponding to the (110), (220), (311), and (400) planes, respectively. These peaks are characteristic of Bragg's reflection based on the face-centered cubic (FCC) crystal structure of EC-Fe_3O_4NPs, in accordance with the JCPDS standard data (11-0614). No additional diffraction peaks were detected other than those corresponding to Fe_3O_4NPs. However, the broadening of Bragg's peaks indicates the formation of EC-Fe_3O_4NPs. The XRD pattern thus confirms that the EC-Fe_3O_4NPs synthesized via the reduction of Fe^{3+} ions by EC extracts are crystalline in nature.

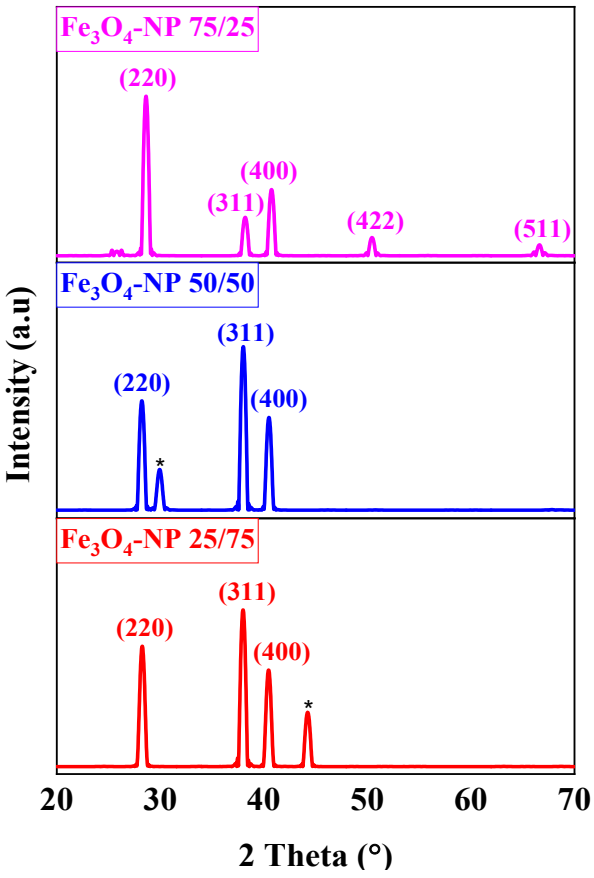

Figure 2. XRD of patterns of Fe_3O_4-NPs synthesized at different amount of the reducing agent and the metal salt solution.

3.5. Scanning electron spectroscopy (SEM) and energy dispersive X-ray (EDX) analysis

Surface morphological studies of EC-Fe_3O_4 NPs were performed using scanning electron microscopy (SEM), and elemental analysis was obtained using EDX. As shown in Figure 3e, the Fe_3O_4 nanoparticles are uniformly embedded in the EC matrix and remain stable with minimal aggregation, which is consistent with Figures 3f and 3g.

Therefore, the issue arising from magnetic dipole-dipole interactions between Fe_3O_4 nanoparticles appears to be resolved due to their dispersion within the EC matrix. Figure 3a presents a typical EDX analysis of EC-Fe_3O_4 NPs. The peaks around 0.5, 1, and 2.01 keV indicate that only oxygen (O), carbon (C), and iron (Fe) elements are present in the sample. The strong energy signal peak for Fe atoms around 2.01 keV is characteristic of metallic Fe nanocrystals, with EC acting as a reductant and capping agent. The strong single energy peak indicates the purity of Fe (77.85%) in the sample, while other studies have reported the presence of C (3.22%) and O (20.02%) in synthesized Fe_3O_4 NPs.

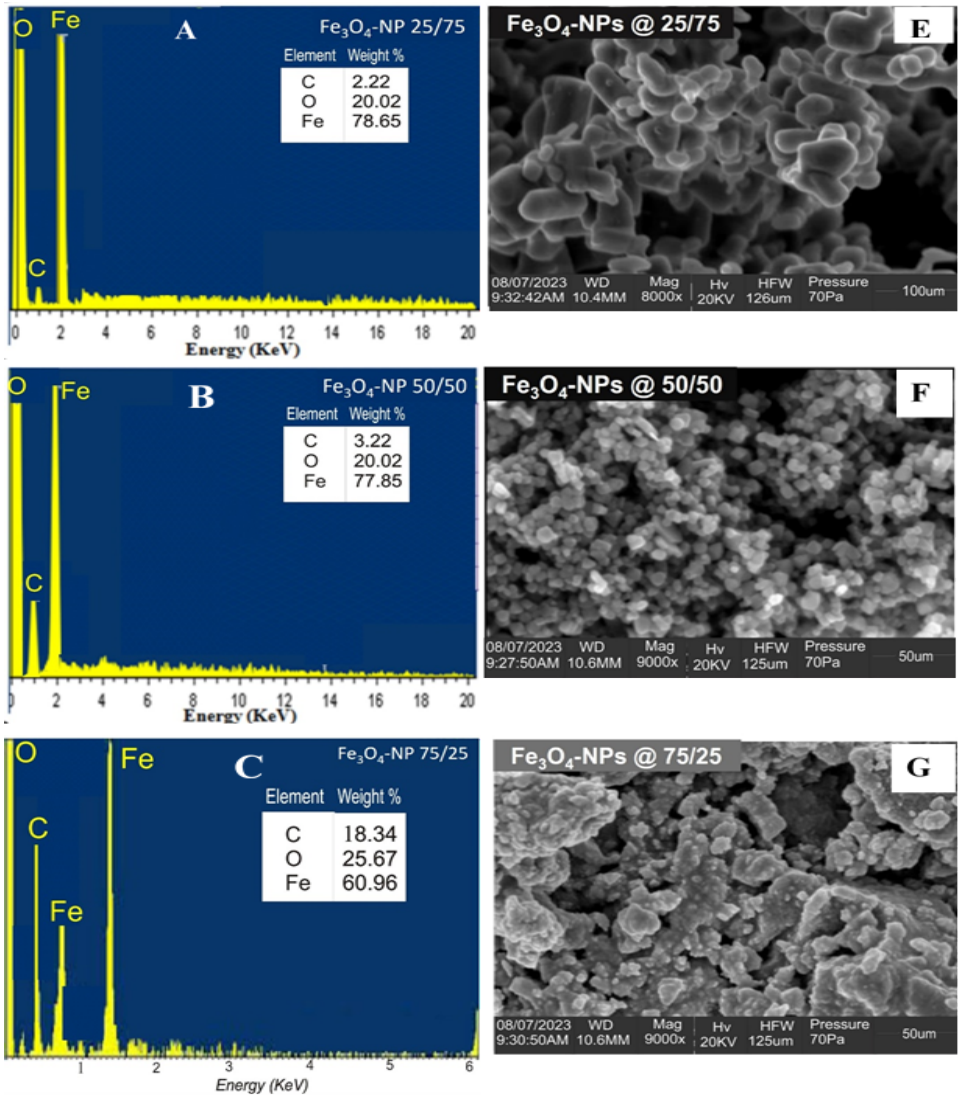

Figure 3. SEM Images and EDX plot of the Fe_3O_4-NPs.

3.6. Transmission electron microscopy and particle size distribution

In the assessment of the morphology and size of the synthesized EC-Fe_3O_4 nanoparticles, a transmission electron microscope (TEM) and a particle size analyzer were used. Figures 4a, 4b, and 4c represent TEM images of EC-Fe_3O_4 at different concentrations. As shown in these figures, the Fe_3O_4 nanoparticles exhibit a nanocrystalline structure, and their shape is approximately spherical.

Furthermore, a careful review of these images reveals that the EC-Fe_3O_4 nanoparticles tend to agglomerate due to their high surface area and the magnetic dipole-dipole interactions between them, as compared to Fe nanoparticles. To determine the mean size of the spherical EC-Fe_3O_4 nanoparticles, we obtained the histogram of the particle size distribution, as shown in Figures 4e, 4f, and 4g. The graphical results in these figures indicate that the sizes of the EC-Fe_3O_4 nanoparticles range from 1.6 to 30 nm, with an average particle size of 15.03 ± 7.39 nm.

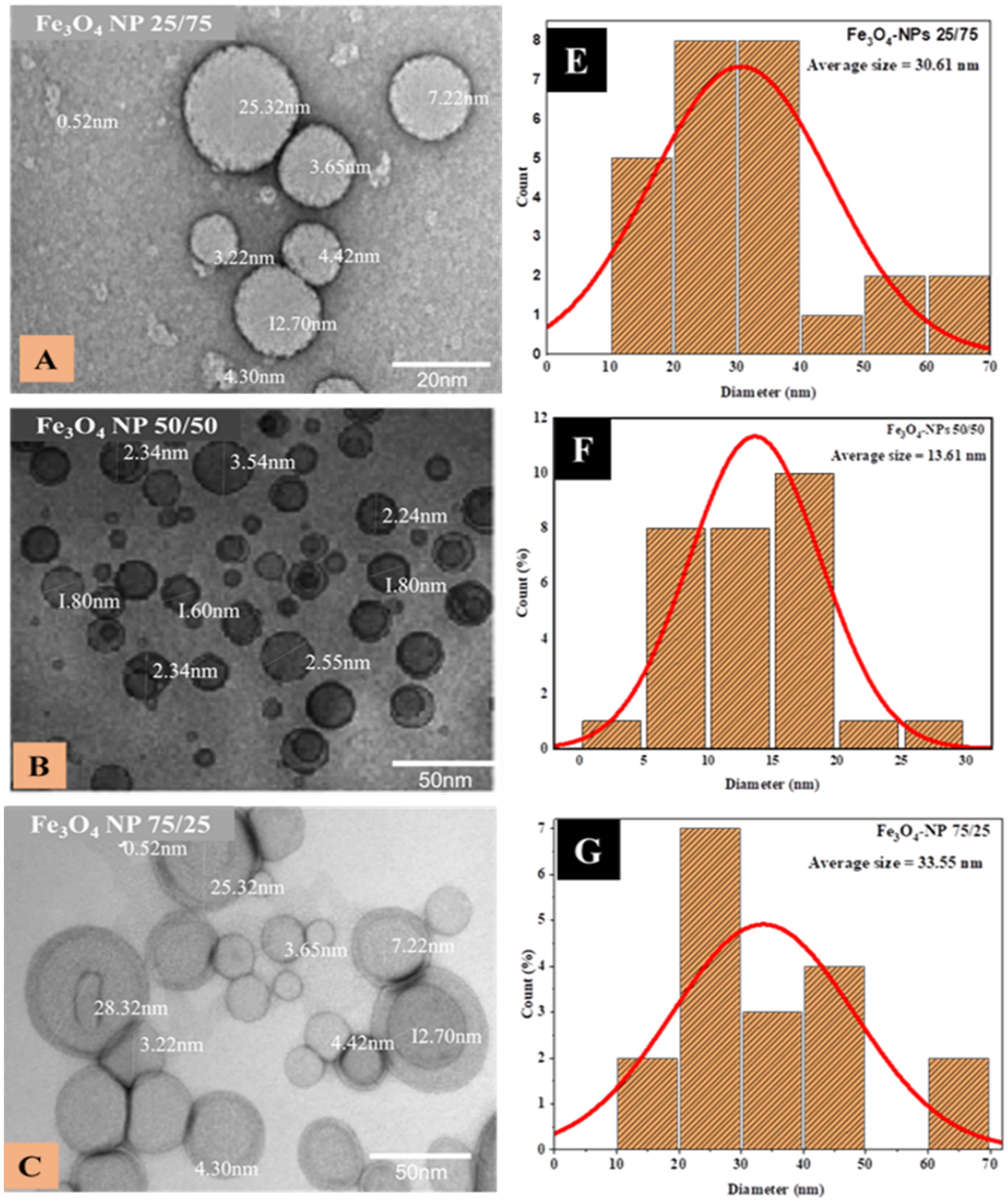

Figure 4. TEM micrographs and Average particle size histogram of the Fe_3O_4NPs.

3.7. Radical scavenging activity of the Fe_3O_4NPs

Antioxidant Activity

In this study, DPPH radical-scavenging activity was measured to identify the antioxidant activity of EC Fe Nano 25/75, EC Fe Nano 50/50, and EC Fe Nano 75/25 extracts. The DPPH radical-scavenging activity (%) of EC 25/75 Nano increased as the concentration increased from 10, 20, 30, 40, and 50 µL/mL, with values of 24, 39, 47, 55, and 73%, respectively. For EC 50/50 Nano, the values were 31, 32, 39, 47, and 63%. Summing up these data, this study concluded that water is the most suitable solvent to enhance radical-scavenging activity. The study results show that the EC Fe Nano 25/75 aqueous extract exhibited the highest DPPH radical-scavenging activity (73%), followed by EC Fe 50/50 (63%) and EC Fe 75/25 (68%). The antioxidant activity of the extracts also proportionally increased in the water extract. Turmeric leaf ethanol extract (1 mg/mL concentration) showed higher DPPH radical-scavenging activity (80.11%) than the water extract (74.65%). There was also a significant difference in the radical-scavenging activity between the ethanol extract and the water extract, similar to the pattern observed in DPPH radical-scavenging activity. However, this indicates only a slight difference, and we concluded that this distinction may be due to differences in solvent concentration.

3.8. Antimicrobial studies of the Fe_3O_4NPs

EC Fe 75/25 exhibits lower antimicrobial inhibition compared to the 25/75 nanoparticles. The inhibition trend is similar for all pathogens except *K. pneumoniae*, which shows the least inhibition among the 50/50 EC Fe samples. The inhibition pattern remains consistent for most pathogens, except for *S. typhi* and *K. pneumoniae*, which display the lowest inhibition across all EC Fe samples. The maximum inhibition observed is 20 mm, while the minimum is 5 mm. Increasing the material concentration generally results in higher inhibition for four organisms, whereas *K. pneumoniae* follows a different trend, showing the highest inhibition at a concentration of 200 µg/L.

The increase in material concentration results in higher inhibition for five organisms. EC Fe 50/50 shows a different trend, with the highest inhibition at a concentration of 400 µg/L and weak inhibition at 50 µg/L. EC Fe 75/25 exhibits very weak inhibition at concentrations below 100 µg/L. The maximum inhibition was observed at 12 mm for a nanoparticle concentration of 400 µg/L.

Susceptibility test of the various

The EC plant extract shows activity against *S. aureus*, *Streptococcus pneumoniae*, *E. coli*, *Salmonella typhi*, and *Klebsiella pneumoniae*. According to the World Health Organization (WHO) report on infectious diseases, overcoming antibiotic resistance is a major challenge for the WHO in the coming millennium. Hence, the last decade has witnessed an increase in the investigation of plants as a source for human disease management. This study shows that the investigation of plants as a source of antimicrobial agents was enhanced by increasing the concentration of the extract.

The activities of the plant extracts are ranked as follows: EC plant extract silver ranked first, followed by EC Fe Nano 25/75, EC Fe Nano 50/50, and EC Fe Nano 75/25 in second, third, and fourth places, respectively. Based on the organism, *Staphylococcus aureus* and *Escherichia coli* were found to be more sensitive to the extracts.

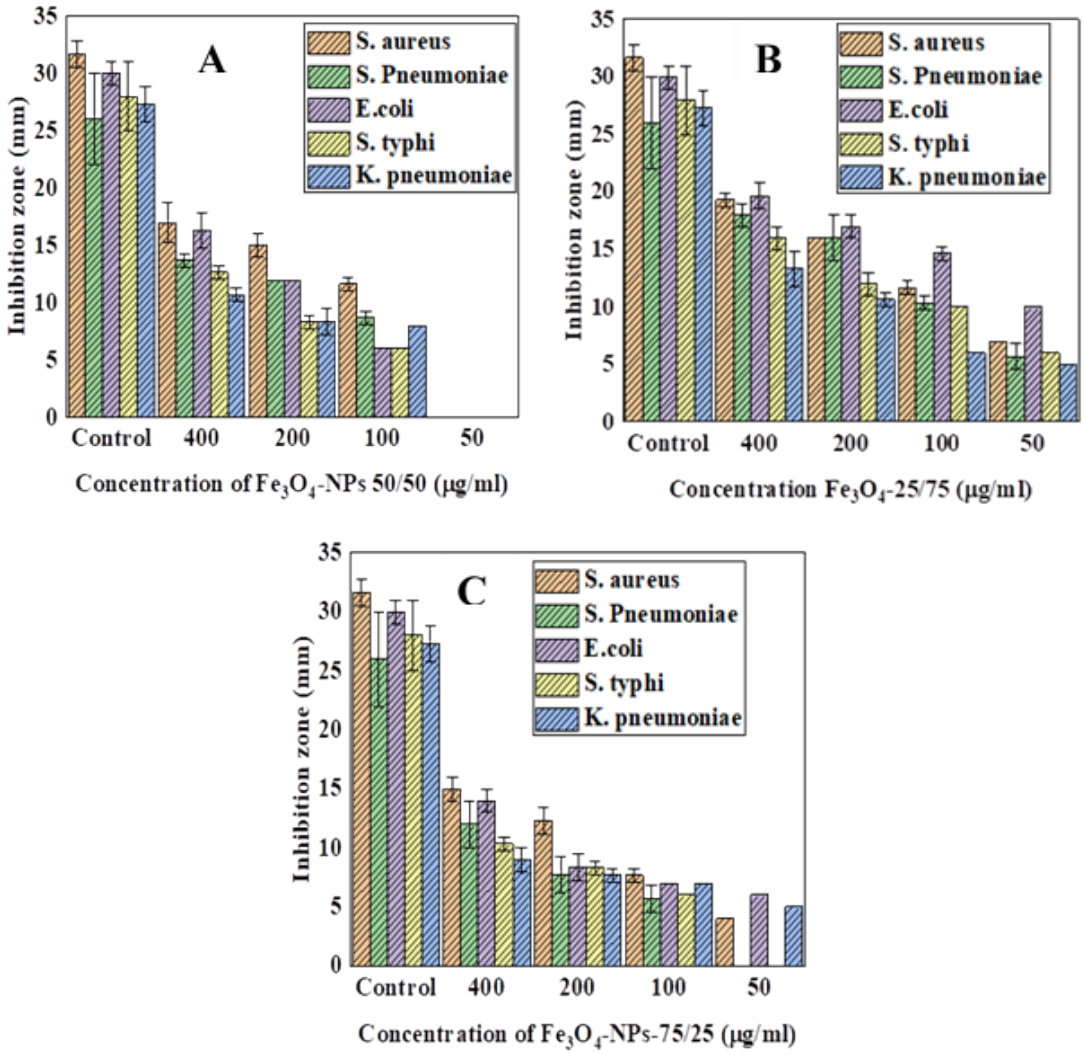

Figure 5. Graph of antimicrobial activity of Fe3O4-NP-25/75 (A), Fe3O4-NP-50/50 (B), Fe3O4-NP-75/25 (C).

Conclusion

This study successfully reports the synthesis of FeNPs, as confirmed by FTIR, SEM-EDX, XRD, and UV-Spectrophotometry. FTIR analysis confirmed the presence of carbohydrate groups from the plant extract on the synthesized FeNPs. The characteristic peaks of FeNPs were observed in the XRD plots of the synthesized nanoparticles. The proximate composition revealed that water hyacinth has both nutritional and medicinal value.

The antioxidant study shows that FeNPs exhibit good scavenging activity, with the highest percentages recorded at 63% and 71%. DPPH free-radical scavenging activity tests were conducted to evaluate the antioxidant potential of the FeNP extracts, and the results indicated varying degrees of scavenging activity among different extracts, with FeNPs 25/75 demonstrating the highest activity.

Antimicrobial tests showed that the synthesized nanoparticles exhibited inhibitory effects against various pathogens, with inhibition zones increasing at higher nanoparticle concentrations. The efficacy of the nanoparticles varied depending on their composition and concentration, with EC Fe Nano and Fe Nano 25/75 demonstrating the highest inhibitory effects. The reusability study of these materials revealed that EC Fe Nano 25/75 was more stable compared to FeNPs 75/25.

References

[1] Mbachu, C. A., Babayemi, A. K., Egbosiuba, T. C., Ike, J. I., Ani, I. J., & Mustapha, S. (2023). Green synthesis of iron oxide nanoparticles by Taguchi design of experiment method for effective adsorption of methylene blue and methyl orange from textile wastewater. *Results in Engineering, 19*, 101198. https://doi.org/10.1016/j.rineng.2023.101198

[2] Irshad, M. A., Nawaz, R., Wojciechowska, E., Mohsin, M., Nawrot, N., Nasim, I., & Hussain, F. (2023). Application of nanomaterials for cadmium adsorption for sustainable treatment of wastewater: A review. *Water, Air, & Soil Pollution, 234*(1), 54. https://doi.org/10.1007/s11270-023-06064-7

[3] Alfieri, A., Anantharaman, S. B., Zhang, H., & Jariwala, D. (2023). Nanomaterials for quantum information science and engineering. *Advanced Materials, 35*(27), 2109621. https://doi.org/10.1002/adma.202109621

[4] Winkler, R., Ciria, M., Ahmad, M., Plank, H., & Marcuello, C. (2023). A review of the current state of magnetic force microscopy to unravel the magnetic properties of nanomaterials applied in biological systems and future directions for quantum technologies. *Nanomaterials, 13*(18), 2585. https://doi.org/10.3390/nano13182585

[5] Sharma, M., Das, P. P., & Purkait, M. K. (2023). Energy storage properties of nanomaterials. In *Advances in smart nanomaterials and their applications* (pp. 337-350). Elsevier. https://doi.org/10.1016/B978-0-323-99546-7.00005-7

[6] Uwaya, G. E., Fayemi, O. E., Sherif, E. S. M., Junaedi, H., & Ebenso, E. E. (2020). Synthesis, electrochemical studies, and antimicrobial properties of Fe_3O_4 nanoparticles from Callistemon viminalis plant extracts. *Materials, 13*(21), 4894. https://doi.org/10.3390/ma13214894

[7] Yusefi, M., Shameli, K., Su Yee, O., Teow, S. Y., Hedayatnasab, Z., Jahangirian, H., & Kuča, K. (2021). Green synthesis of Fe_3O_4 nanoparticles stabilized by a Garcinia mangostana fruit peel extract for hyperthermia and anticancer activities. *International Journal of Nanomedicine, 16*, 2515-2532. https://doi.org/10.2147/IJN.S284134

[8] Sathishkumar, G., Logeshwaran, V., Sarathbabu, S., Jha, P. K., Jeyaraj, M., Rajkuberan, C., & Sivaramakrishnan, S. (2018). Green synthesis of magnetic Fe_3O_4 nanoparticles using Couroupita guianensis Aubl. fruit extract for their antibacterial and cytotoxicity activities. *Artificial Cells, Nanomedicine, and Biotechnology, 46*(3), 589-598. https://doi.org/10.1080/21691401.2017.1332635

[9] Ramesh, A. V., Rama Devi, D., Mohan Botsa, S., & Basavaiah, K. (2018). Facile green synthesis of Fe_3O_4 nanoparticles using aqueous leaf extract of Zanthoxylum armatum DC. for efficient adsorption of methylene blue. *Journal of Asian Ceramic Societies, 6*(2), 145-155. https://doi.org/10.1080/21870764.2018.1459335

[10] Karami, N., Mohammadpour, A., Samaei, M. R., Amani, A. M., Dehghani, M., Varma, R. S., & Sahu, J. N. (2024). Green synthesis of sustainable magnetic nanoparticles Fe_3O_4 and Fe_3O_4-chitosan derived from Prosopis farcta biomass extract and their performance in the sorption of lead (II). *International Journal of Biological Macromolecules, 254*, 127663. https://doi.org/10.1016/j.ijbiomac.2023.127663

[11] Ghoohestani, E., Samari, F., Homaei, A., & Yosuefinejad, S. (2024). A facile strategy for preparation of Fe_3O_4 magnetic nanoparticles using Cordia myxa leaf extract and investigating its adsorption activity in dye removal. *Scientific Reports, 14*(1), 84. https://doi.org/10.1038/s41598-023-50550-1

[12] Zakernezhad, F., Rasekh, B., Yazdian, F., & Maghami, P. (2024). The role of surface modification of silica-coated Fe_3O_4 nanoparticles in the structure and enzyme activity of lysozyme. *BioNanoScience*, 1-14. https://doi.org/10.1007/s12668-024-01298-z

[13] Abdelmonem, M., Albert, E. L., Alhadad, M. A., & Abdullah, C. A. (2024). Plant-polyphenol-mediated synthesis of magnetic biocompatible iron oxide nanoparticles for diagnostic imaging and management of neurodegenerative diseases. Precision Nanomedicine, 1233-1251. https://doi.org/10.33218/001c.92424

[14] Nozhat, Z., Wang, S., Mushtaq, A., Deng, T., Iqbal, M. Z., & Kong, X. (2024). Temozolomide loaded Fe_3O_4@SiO_2 nanoparticles for MR-imaging directed synergistic therapy of glioblastoma multiforme in vitro. *Materials Today Communications*, 108289. https://doi.org/10.1016/j.mtcomm.2024.108289

[15] Phumying, S., Labuayai, S., Thomas, C., Amornkitbamrung, V., Swatsitang, E., & Maensiri, S. (2013). Aloe vera plant-extracted solution hydrothermal synthesis and magnetic properties of magnetite (Fe_3O_4) nanoparticles. *Applied Physics A, 111*, 1187-1193. https://doi.org/10.1007/s00339-012-7340-5

[16] Mitchell, E., De Souza, F., Gupta, R. K., Kahol, P. K., Kumar, D., Dong, L., & Gupta, B. K. (2015). Probing on the hydrothermally synthesized iron oxide nanoparticles for ultra-capacitor applications. *Powder Technology, 272*, 295-299. https://doi.org/10.1016/j.powtec.2014.12.021

[17] Khan, S. R., Jamil, S., Janjua, M. R. S. A., & Khera, R. A. (2017). Synthesis of ferric oxyhydroxide nanoparticles and ferric oxide nanorods by reflux-assisted coprecipitation method and comparative study of their thermal properties. *Materials Research Express, 4*(11), 115019. https://doi.org/10.1088/2053-1591/aa971e

[18] Mohammed, S. A. J., Al-Rawi, B. K., & Al-Haddad, R. M. (2023). Fe_3O_4@SiO_2 core-shell nanoparticles: Synthesis, characterization prepared by green method for Iraqi Aloe vera extract. *International Journal of Nanoscience, 22*(02), 2350009. https://doi.org/10.1142/S0219581X23500096

[19] Tovar, G. I., Briceño, S., Suarez, J., Flores, S., & González, G. (2020). Biogenic synthesis of iron oxide nanoparticles using Moringa oleifera and chitosan and its evaluation on corn germination. *Environmental Nanotechnology, Monitoring & Management, 14*, 100350. https://doi.org/10.1016/j.enmm.2020.100350

[20] Sari, I. P., & Yulizar, Y. (2017, April). Green synthesis of magnetite (Fe_3O_4) nanoparticles using Graptophyllum pictum leaf aqueous extract. In *IOP Conference Series: Materials Science and Engineering* (Vol. 191, No. 1, p. 012014). IOP Publishing. https://doi.org/10.1088/1757-899X/191/1/012014

[21] Ramesh, A. V., Rama Devi, D., Mohan Botsa, S., & Basavaiah, K. (2018). Facile green synthesis of Fe_3O_4 nanoparticles using aqueous leaf extract of Zanthoxylum armatum DC. for efficient adsorption of methylene blue. *Journal of Asian Ceramic Societies, 6*(2), 145-155. https://doi.org/10.1080/21870764.2018.1459335

[22] Salem, D. M., Ismail, M. M., & Aly-Eldeen, M. A. (2019). Biogenic synthesis and antimicrobial potency of iron oxide (Fe_3O_4) nanoparticles using algae harvested from the Mediterranean Sea, Egypt. *The Egyptian Journal of Aquatic Research, 45*(3), 197-204. https://doi.org/10.1016/j.ejar.2019.07.002

[23] Mousavi, S. M., Hashemi, S. A., Ramakrishna, S., Esmaeili, H., Bahrani, S., Koosha, M., & Babapoor, A. (2019). Green synthesis of supermagnetic Fe_3O_4-MgO nanoparticles via Nutmeg essential oil toward superior anti-bacterial and anti-fungal performance. *Journal of Drug Delivery Science and Technology, 54,* 101352. https://doi.org/10.1016/j.jddst.2019.101352

[24] Cai, L., Cai, L., Jia, H., Liu, C., Wang, D., & Sun, X. (2020). Foliar exposure of Fe_3O_4 nanoparticles on Nicotiana benthamiana: Evidence for nanoparticles uptake, plant growth promoter, and defense response elicitor against plant virus. *Journal of Hazardous Materials, 393*, 122415. https://doi.org/10.1016/j.jhazmat.2020.122415

[25] Alexeree, S. M., Abou-Seri, H. M., El-Din, H. E. S., Youssef, D., & Ramadan, M. A. (2024). Green synthesis of silver and iron oxide nanoparticles mediated photothermal effects on Blastocystis hominis. *Lasers in Medical Science, 39*(1), 43. https://doi.org/10.1007/s10103-024-03984-6

[26] Shelar, A., Didwal, P. N., & Patil, R. (2024). Recent advances in antifungal nanomaterials for combating biofilm infection caused by Candida albicans. In *Applications of nanotechnology in microbiology* (pp. 271-290). Springer. https://doi.org/10.1007/978-3-031-49933-3_10

[27] Kale, S. S., Chauhan, R., Nigam, B., Gosavi, S., & Chaudhary, I. J. (2024). Effectiveness of nanoparticles in improving soil fertility and eco-friendly crop resistance: A comprehensive review. *Biocatalysis and Agricultural Biotechnology*, 103066. https://doi.org/10.1016/j.bcab.2024.103066

[28] Ikhuoria, E. U., Uwidia, I. E., Okojie, R. O., Ifijen, I. H., & Chikaodili, I. D. (2024). Synergistic antibacterial action of iron, silver, and vanadium ternary oxide nanoparticles: Green mediated synthesis using tailored plant extract blends. *Biomedical Materials & Devices*, 1-19. https://doi.org/10.1007/s44174-024-00162-8

[29] Sullivan, P. R., & Wood, R. (2012, October). Water hyacinth (Eichhornia crassipes (Mart.) Solms) seed longevity and the implications for management. In *Eighteenth Australasian Weeds Conference* (Vol. 1933, pp. 37-40). Weed Society of Victoria Inc.

[30] Pendse, D. S., & Deshmukh, M. P. (2024). A comprehensive study on an integrated approach for water hyacinth management to conserve natural water resources in India. *Materials Today: Proceedings*. https://doi.org/10.1016/j.matpr.2023.12.047

[31] Ayanda, O. I., Ajayi, T., & Asuwaju, F. P. (2020). Eichhornia crassipes (Mart.) Solms: Uses, challenges, threats, and prospects. *The Scientific World Journal, 2020*, 3452172. https://doi.org/10.1155/2020/3452172

[32] Sandeep, P., Neha, S., Nirala, A. K., & Anup, G. (2015). Dynamics of water weed Eichhornia crassipes: A review. *International Journal for Research in Applied Science and Engineering Technology, 3*(10), 137-140.

[33] Lalitha, P., & Jayanthi, P. (2014). Antiaging activity of the skin cream containing ethyl acetate extract of Eichhornia crassipes (Mart.) Solms. https://doi.org/10.1155/2014/943287

[34] Aboul-Enein, A. M., Shanab, S. M., Shalaby, E. A., Zahran, M. M., Lightfoot, D. A., & El-Shemy, H. A. (2014). Cytotoxic and antioxidant properties of active principals isolated from water hyacinth against four cancer cell lines. *BMC Complementary and Alternative Medicine, 14*(1), 1-11. https://doi.org/10.1186/1472-6882-14-397

[35] Aida, P., Rosa, V., Blamea, F., Tomas, A., & Salvador, C. (2001). Paraguayan plants used in traditional medicine. *Journal of Ethnopharmacology, 16*, 93-98. https://doi.org/10.1016/S0378-8741(01)00214-8

[36] Sud, D., & Kaur, P. (2011). Heterogeneous photocatalytic degradation of selected organophosphate pesticides: A review. *Critical Reviews in Environmental Science and Technology, 42*(22), 2365-2407. https://doi.org/10.1080/10643389.2011.574184